$2s_{1/2}$ occupancies in ^{30}Si, ^{31}P, and ^{32}S

J. Wesseling, C. W. de Jager, L. Lapikás, and H. de Vries
Nationaal Instituut voor Kernfysica en Hoge-Energie Fysica (NIKHEF), P.O. Box 41882, NL-1009 DB Amsterdam, The Netherlands

L. W. Fagg
The Catholic University of America, Washington, D.C. 20064

M. N. Harakeh and N. Kalantar-Nayestanaki
KVI, Zernikelaan 25, NL-9747 AA Groningen, The Netherlands

R. A. Lindgren
University of Virginia, Charlottesville, Virginia 22901

E. Moya De Guerra and P. Sarriguren
I.E.M., C.S.I.C., Serrano 119, E-28006 Madrid, Spain
(Received 10 December 1996)

Elastic electron scattering off ^{30}Si and ^{31}P was studied in an effective momentum-transfer range of 1.8–3.0 fm^{-1}. The form-factor data were analyzed together with existing data sets for these nuclei and for ^{32}S in a model-independent Fourier-Bessel expansion. For ^{31}P the $M1$ contribution was subtracted following an established parametrization. Results of Hartree-Fock (HF) calculations, performed for these three nuclei in a spherical basis and in an axially deformed basis, are compared to experiment. Occupancies have been determined which, when used in the spherical-basis HF calculations, lead to a good description of the elastic form-factor data. The deformed-basis calculations have been used to study the influence of the deformation on the calculated binding energies and ground-state charge densities. In all calculations the influence of using different effective nucleon-nucleon interactions was investigated. The resulting differences in $2s_{1/2}$ in occupancy are combined with results from previous existing $(e,e'p)$ experiments to yield ''absolute occupancies'' for the $2s_{1/2}$ orbital. The deduced $2s_{1/2}$ occupancies for ^{30}Si and ^{32}S are 0.24(4) and 1.35(19), respectively. [S0556-2813(97)01306-X]

PACS number(s): 21.10.Ft, 25.30.Bf, 21.60.Jz, 27.30.+t

I. INTRODUCTION

The occupancy of valence shells has, over the years, been studied with a variety of probes, all having their own specific properties. Occupancies deduced for many nuclei from magnetic electron scattering, where the spin magnetic moments of the valence-shell particles are probed, have proved to be quite model dependent [1]. Spectroscopic factors obtained with pickup reactions, such as the $(d,^3\mathrm{He})$ reaction, on the other hand, have proved to be rather sensitive [2] to the rms radius of the employed bound-state wave function (BSWF), a quantity that cannot be measured with pickup reactions. This encumbers the absolute determination of spectroscopic factors through pickup reactions. Over the past 15 years electron-induced proton knockout $(e,e'p)$ has also been employed to study the distribution of nucleons over nuclear orbitals [3]. All basic ingredients in the extraction of spectroscopic factors from $(e,e'p)$ experiments are at present reasonably well understood [4], and furthermore the electron-proton coupling in the nuclear medium and the effects of electron distortion have been investigated [5,6].

An important advantage of the $(e,e'p)$ reaction is that the rms radius of the BSWF can be measured directly [4]. The spectroscopic factors, extracted with this method, are not very sensitive to the shape of the single-particle (s.p.) binding potential or to the optical-model potential describing the scattering of the outgoing proton. Hence, these ''absolute'' values are free from the normalization uncertainties, encountered in the analysis of $(d,^3\mathrm{He})$ experiments. Furthermore, it should be emphasized that the analysis of both the $(d,^3\mathrm{He})$ reaction and the $(e,e'p)$ reaction does not yield occupancies but spectroscopic factors. These spectroscopic factors are essentially a measure of the overlap between the initial state of the target nucleus probed, generally its ground state, and the final state. The latter state consists of the $(A-1)$ daughter nucleus (possibly in an excited state) and the outgoing proton.

The first values for spectroscopic factors obtained with the $(e,e'p)$ reaction were small compared to results obtained with the $(d,^3\mathrm{He})$ reaction on the same nuclei. A thorough study of the analyses performed in $(d,^3\mathrm{He})$ and $(e,e'p)$ reactions has, however, shown that the spectroscopic factors obtained with the $(d,^3\mathrm{He})$ reaction were too high. A reanalysis [2] of the $(d,^3\mathrm{He})$ data, using the same BSWF in the analysis as determined from $(e,e'p)$ experiments, resulted in a reasonable agreement between spectroscopic factors deduced from both reactions. The resulting values are on average 60–70 % of the valence-shell spectroscopic factors expected on the basis of the independent-particle shell model (IPSM). This is observed for nuclei all over the periodic table [7].

It is now believed that (short-range) nuclear correlations

[8,9] are responsible for this depletion of the valence shells. They are found to induce a fragmentation of the spectroscopic strength and, furthermore, to shift part of the strength into the energy region above 200 MeV, well outside the energy range covered by present experiments. Sophisticated theoretical calculations [10–12] reproduce the observed spectroscopic data reasonably well in a number of nuclei.

In order to estimate *occupancies* from the measured *spectroscopic factors*, the combined evaluation of relative spectroscopic factors and electron scattering (CERES) method [13] has been proposed. This method connects the ratio of integrated spectroscopic strengths, obtained for knockout from a specific shell, in nuclei A and $(A+k)$ to the ratio of proton occupancies in this shell [14,15] in both nuclei. The experimental charge-density difference between these nuclei can be related to a proton-occupancy-number difference by means of a Hartree-Fock (HF) calculation.

The CERES method has been used previously [13,16,17] in the case of the $3s_{1/2}$ shell in the Pb region as the wave function of protons in $s_{1/2}$ shells has a unique radial signature. In those studies the sensitivity of the calculated occupancy differences to the use of different effective interactions in the HF calculations was not extensively investigated. However, it was shown [18,19] that the derivation of the $3s_{1/2}$ occupancy difference between ^{205}Tl and ^{206}Pb is subject to ambiguities and is, furthermore, sensitive to the specific nucleon-nucleon interaction used in its determination.

In a previous HF study of sd-shell nuclei [20] neither elastic form-factor data nor occupancies (different from the IPSM values) were considered. For ^{32}S there is already an extensive data set. For ^{30}Si and ^{31}P, however, the existing data sets are of limited range or accuracy.

In the present paper, we present elastic electron-scattering data for the nuclei ^{30}Si and ^{31}P. These data make it possible, in combination with existing data sets, to map the elastic form factor up to relatively high values of the effective [21] momentum transfer ($q_{\rm eff}$=3.0 fm^{-1}). These form-factor data, combined with the extensive data that already exist for ^{32}S, are used to determine the ground-state occupancy numbers for ^{30}Si, ^{31}P, and ^{32}S. Since many sd-shell nuclei are known to be deformed [20,22], two sets of HF calculations are performed, one in a spherical basis and one in a deformed basis. The resulting $2s_{1/2}$-occupancy differences are combined with the integrated spectroscopic strengths obtained for the same nuclei in previous $(e,e'p)$ experiments [23] to yield $2s_{1/2}$ occupancies.

Transitions resulting from knockout from the $2s_{1/2}$ orbital have a characteristic momentum distribution, quite distinct from distributions observed for knockout from neighboring orbitals. Therefore, for application of the CERES method the summed spectroscopic strength could be determined unambiguously enough only for knockout from the $2s_{1/2}$ orbital; for other orbitals, the contribution from the spin-orbit partners could not be separated.

II. EXPERIMENTAL DETAILS AND DATA ANALYSIS

The experiments presented in this paper were performed at the NIKHEF medium-energy accelerator (MEA) [24]. Self-supporting disks of silicon, phosphor, and lithium-sulfide were used as targets. The silicon target, enriched in ^{30}Si, contained 9% ^{16}O and CH binder. The phosphor target consisted of black natural ^{31}P, without measurable contaminants. Since it was not possible to make a target of pure sulfur with the required thickness (roughly 25 mg/cm^2) and dimensions (diameter larger than 1.0 cm) that could withstand an average beam current of several μA, Li_2S was used as target material. For the ^{30}Si, ^{31}P, and ^{32}S measurements maximum average currents of 15 μA, 7.5 μA, and 6 μA, respectively, were used, while the targets were rotated continuously.

TABLE I. Scattering angles, effective momentum transfers, cross sections, and statistical uncertainties for the data obtained in the present experiment at E_e=454.3 MeV.

$\theta_{\rm lab}$ [deg]	$q_{\rm eff}$ [fm^{-1}]	$\sigma_{\rm expt}$ [fm^2/sr]	$\Delta\sigma_{\rm expt}$ [%]
^{30}Si			
60.45	2.350	0.53×10^{-8}	6.0
63.20	2.445	1.24×10^{-8}	7.4
66.10	2.544	1.67×10^{-8}	6.0
70.22	2.681	1.42×10^{-8}	7.0
73.86	2.800	8.11×10^{-9}	6.5
78.61	2.950	2.56×10^{-9}	10.3
^{31}P			
55.50	2.178	0.98×10^{-7}	3.4
62.62	2.428	2.11×10^{-9}	3.9
63.77	2.468	3.01×10^{-8}	3.8
65.53	2.528	2.80×10^{-8}	3.4
66.67	2.567	2.57×10^{-8}	2.4
68.69	2.634	1.72×10^{-8}	3.6
69.83	2.672	2.16×10^{-8}	4.8

The energy of the incident electrons was 454.3 MeV. For normalization purposes initial scattering angles were chosen such that $q_{\rm eff}$ was 1.6 fm^{-1}, close to the second diffraction maximum for elastic scattering off ^{12}C, where accurate data are available [25]. Two short ^{32}S measurements were performed to ensure a consistent (energy) normalization of the present data with respect to the existing data sets. Scattering angles, effective momentum transfers, and experimental cross sections are listed in Table I.

At the relatively high $q_{\rm eff}$ values measured in the present work, the count rates are quite low. Kinematical broadening of the spectra was corrected for using the well-known optical properties of the magnetic QDD spectrometer [26]. This procedure results in a dramatic improvement of the energy resolution. In Fig. 1 two ^{31}P spectra are shown, one before and one after the corrections have been applied. The cross sections were subsequently determined with the code ALLFIT [27] by fitting the spectra with an asymmetric Gaussian, folded with a theoretical function for the radiation tail.

A simultaneous model-independent analysis of the present and older data sets (listed in Table II) was performed using the code MEFIT [28]. To account for uncertainties in the charge density due to the finite $q_{\rm eff}$ range mapped in the experiments, pseudodata were generated according to the method described in Ref. [29]. The normalizations of different data sets were allowed to vary within a limited range. For ^{30}Si all data sets agree within 2.5%, resulting in a good si-

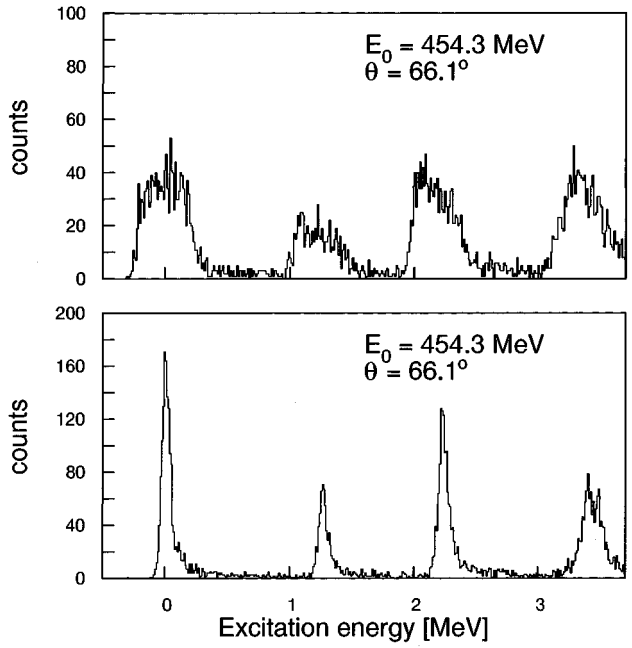

FIG. 1. The top and bottom figures show, respectively, ^{31}P energy spectra before and after off-line software corrections for kinematical broadening and spectrometer aberrations are applied.

multaneous description of the available form-factor data. For ^{31}P there is a complication due to the presence of the $M1$ contribution to the total cross section. To calculate this contribution the parametrization of the $M1$ current given by Ref. [30] was employed. The $C0$ and $M1$ form factors are shown in Fig. 2 for energies of 295, 400, and 454.3 MeV. The cross-section data given in Ref. [28] were not corrected for the $M1$ contribution, although at the low maximum energy and relatively large scattering angles in that experiment the $M1$ form factor is dominant in the region of the second diffraction minimum. After correcting the data of Ref. [28] as well as the present data for the $M1$ contribution both sets are in good agreement. A discrepancy, however, exists with the set of 400 MeV data of Ref. [31], as was already pointed out by Merle [28]. Although these 400 MeV data have reportedly been corrected for the $M1$ contribution, the applied corrections are much smaller than the corrections calculated with the parametrization of the $M1$ current mentioned above. If the $M1$ correction is performed consistently for all data sets, the quality of the fit deteriorates by the inclusion of this 400 MeV data set in the analysis. Also, when the normalization of these latter data is allowed to vary within reasonable limits no consistency could be obtained. Therefore, this data set was not included in the determination of the ground-state charge density.

A similar combined analysis of all data sets available was performed for ^{32}S. Here again the 400 MeV data of Ref. [31] resulted in a deterioration of the description of the data and have therefore not been included in the final analysis. The form-factor data and the Fourier-Bessel fits of the nuclei under study are shown in Fig. 3, and the deduced ground-state charge densities are shown in Fig. 4. Also shown in Fig. 4 is the charge-density difference between ^{32}S and ^{30}Si. This difference shows the characteristic shape of a $2s_{1/2}$ density, but some additional structure is evident which might be attributed to a sizable $1d$ component.

TABLE II. Energies, momentum-transfer ranges, and number of data points for all data sets that were used in the analysis in addition to the data sets given in Table I.

Nucleus	Energy [MeV]	q_{eff} range [fm^{-1}]	Number of data points	Ref.
^{30}Si	100.08	0.27–0.84	11	[30]
	200.11	0.72–1.55	22	
	320.16	1.30–2.64	24	
^{31}P	100.10	0.27–0.81	5	[30]
	200.13	0.81–1.55	10	
	320.14	1.41–2.18	4	
	250.00	0.76–1.83	29	[31]
	400.00	1.19–2.83	25	a
	119.80	0.32–1.27	15	[28]
	199.30	0.97–1.61	10	
	246.30	1.57–1.90	5	
	295.00	0.93–2.50	36	
^{32}S	119.80	0.32–1.27	15	[28]
	199.30	0.98–1.61	10	
	246.30	1.57–1.97	6	
	295.00	0.93–2.51	36	
	250.00	0.76–2.13	35	[33]
	500.00	1.50–3.67	25	
	250.00	0.75–1.84	15	[31]
	400.00	1.19–2.73	13	a
	120.00	0.55–1.00	10	[32]
	120.00	0.50–1.07	14	
	120.00	0.50–1.00	13	
	239.40	0.86–1.77	13	
	320.00	1.14–2.63	15	

[a]Not used in the final analysis, as explained in the text.

The Fourier-Bessel coefficients used in the fitting procedure to parametrize the ground-state charge densities of ^{30}Si, ^{31}P, and ^{32}S are presented in Table III. In the analysis a cutoff radius of 8.0 fm was used. In Ref. [30] it was stated that for ^{30}Si a value of 8.0 fm did not allow a good description of the experimental form-factor data. A value of 8.5 fm resulted in a better description. In the present analysis the Fourier-Bessel coefficients of Ref. [30] for an R_c of 8.5 fm were transformed into a set of Fourier-Bessel (FB) coefficients for an R_c of 8.0 fm. These were subsequently used as starting values in the fit of the data, resulting in a good description of the data.

The rms radii obtained here are in satisfactory agreement with those obtained in previous analyses. For ^{30}Si the rms radius of 3.145(5) fm is somewhat smaller than the value of 3.173(25) fm reported by Ref. [30], although these values are, within the uncertainties, consistent. For ^{31}P the agreement is excellent: A value of 3.191(5) fm is found in the present analysis where 3.190(30) fm, 3.189(10) fm, and 3.187(10) fm are reported by Refs. [31], [28], and [30], respectively. The rms radii obtained with elastic electron scattering, reported for ^{32}S, are 3.248(11) fm [32], 3.245(32) fm [31], 3.239(9) fm [28], and 3.239(30) fm [33]. All these values are compatible with the present value of 3.242(4) fm. It is interesting to note that, although part of the data set used

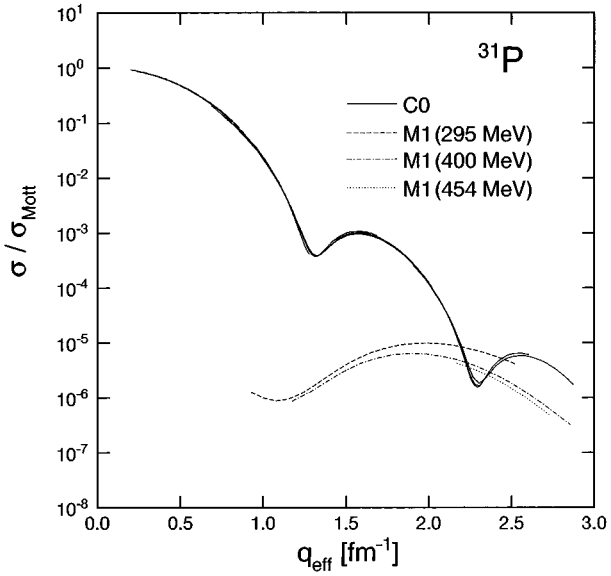

FIG. 2. The calculated $M1$ form factor for ^{31}P for the kinematics of Ref. [28] (dashed line), Ref. [31] (dot-dashed line), and the present experiment (dotted line). These curves have been calculated using the $M1$ current parametrization of Ref. [30]. The solid lines are the fits to the $C0$ form-factor data obtained in the present analysis after subtraction of the $M1$ contributions. The small differences between curves calculated for different energies are caused by distorted-wave Born-approximation (DWBA) corrections.

by Ref. [31] is not compatible with the other data sets, the extracted values of the rms radius agree with each other.

A significant discrepancy is observed when the rms radii measured in electron scattering are compared to those obtained from studies of muonic atoms. For ^{30}Si a rms radius of 3.134(7) fm is reported [34], a value just consistent with the electron-scattering result. Although it is suggested [34]

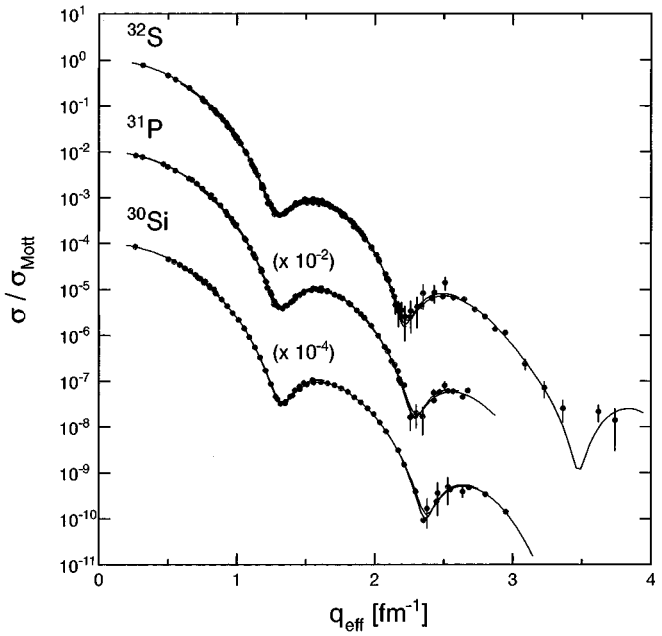

FIG. 3. Form-factor data for ^{32}S, ^{31}P ($\times 10^{-2}$), and ^{30}Si ($\times 10^{-4}$). The solid curves are the Fourier-Bessel fits to the data.

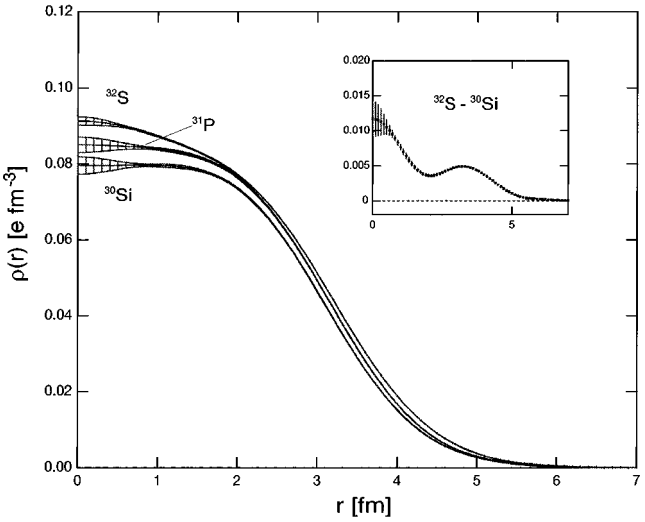

FIG. 4. Ground-state charge distributions, as obtained in the present analysis, for ^{32}S, ^{31}P, and ^{30}Si from top to bottom, respectively. The ground-state charge-density difference between ^{32}S and ^{30}Si is shown separately.

that inconsistencies in absolute normalizations cause rms radii obtained with electron scattering to be mutually incompatible, we have just shown that a consistent analysis *is* possible, as was also demonstrated before [35]. For ^{32}S two values for the rms radius obtained with muonic atoms have been reported: 3.261(1) fm [36] and 3.244(20) fm [37]. The first value is clearly not compatible with any of the (e,e) values discussed above while the latter is. In the determination of the latter value corrections like nuclear polarization have not been taken into account. Comparing the presently deduced difference between the rms radii of ^{30}Si and ^{32}S of 0.098(6) fm to the difference deduced from the values reported by Refs. [34] and [36] of 0.127(7) fm, obtained with muonic atoms, a small but interesting discrepancy emerges.

TABLE III. Fourier-Bessel coefficients for ^{30}Si, ^{31}P, and ^{32}S, as deduced in the present analysis.

	^{30}Si	^{31}P	^{32}S
a_1	3.3161×10^{-2}	3.5280×10^{-2}	3.7282×10^{-2}
a_2	5.6992×10^{-2}	5.9545×10^{-2}	6.0490×10^{-2}
a_3	1.7582×10^{-2}	1.7241×10^{-2}	1.4837×10^{-2}
a_4	-1.7943×10^{-2}	-1.9338×10^{-2}	-1.8600×10^{-2}
a_5	-1.4424×10^{-2}	-1.3171×10^{-2}	-1.0162×10^{-2}
a_6	-2.9131×10^{-4}	1.4065×10^{-3}	2.9785×10^{-3}
a_7	3.7026×10^{-3}	3.6747×10^{-3}	3.8294×10^{-3}
a_8	1.0480×10^{-3}	6.3926×10^{-4}	1.2124×10^{-3}
a_9	-2.5839×10^{-4}	-3.2297×10^{-4}	-2.1994×10^{-4}
a_{10}	3.3079×10^{-5}	1.8286×10^{-4}	-4.4945×10^{-4}
a_{11}	2.7875×10^{-5}	-1.0781×10^{-4}	1.7642×10^{-4}
a_{12}	-3.1252×10^{-5}	6.6628×10^{-5}	-2.5343×10^{-5}
a_{13}	1.8332×10^{-5}	-4.2991×10^{-5}	-3.2039×10^{-5}
a_{14}	-4.3449×10^{-6}	2.8800×10^{-5}	5.0902×10^{-5}
a_{15}	-6.4084×10^{-6}	-1.9932×10^{-5}	-5.3882×10^{-5}
	R_c=8.00 fm	R_c=8.00 fm	R_c=8.00 fm
	r_{rms}=3.145(5) fm	r_{rms}=3.191(5) fm	r_{rms}=3.242(4) fm

The (e,e) values presented here are based on a simultaneous and consistent analysis of a large number of data sets. It is thus quite unlikely that a significant difference in normalization contributes to the rms radii obtained here for ^{30}Si and ^{32}S. The values for the rms radius obtained with muonic atoms, however, have been obtained in independent experiments. It is therefore possible that differences in analysis, such as energy calibration and nuclear polarization corrections, result in a difference in the rms radius that is too large.

With the new data included in the analysis there now exist accurate and mutually consistent elastic form-factor data for all three nuclei ^{30}Si, ^{31}P, and ^{32}S, extending up to $q_{\rm eff}\approx 3$ fm^{-1}. Furthermore, it has been possible to deduce accurate ground-state charge densities and rms radii.

III. HARTREE-FOCK CALCULATIONS

A. Introduction

A possible procedure to obtain information on the occupancy probabilities of shells in a nucleus includes a Hartree-Fock (HF) [38–42] calculation, taking into account the residual pairing interaction by means of a set of estimates for the occupancy probabilities. The calculated observables, which are sensitive to these occupancies, are subsequently compared to experimentally deduced ones. If experimental and calculated values disagree, the occupancies are adjusted to yield a better description. These steps are repeated until the ''best fit'' solution is obtained. In practice this procedure may not be as trivial as it seems.

In using elastic electron-scattering data to estimate occupancies, one is immediately confronted with the choice of observables. If one chooses the experimental charge density, which can essentially be derived in a model-independent way from the measured form-factor data, the error envelope deduced for the experimental charge density is, although model independent, not unambiguous. It has been shown by Dreher *et al.* [29] that, due to the finite $q_{\rm eff}$ range and the correlation between the FB coefficients, not all possible curves within the error envelope correspond to acceptable charge densities. In practice, the situation is less troublesome, provided that the HF calculations yield charge densities that are sufficiently smooth, i.e., that they do not show unphysical wiggles near the nuclear center, which is the region where the problem outlined above is most prominent. On the other hand, these problems are not encountered when cross-section values derived from the calculated charge density are compared to the data.

Another problem arises when one is interested in the difference in occupancy of a certain orbital in two adjacent nuclei. Several combinations of the experimental data can now be used as input to the fitting procedure. The most straightforward procedure is to fit the occupancies to the form-factor data of the two nuclei independently and subsequently take the difference of the deduced occupancies. However, quite often the calculations do not describe the form-factor data (or extracted charge densities) of either nucleus. Therefore, one alternatively tries to describe either the experimental charge-density difference [19] or the experimental form-factor ratio [16,17]. If the observables in neither of the nuclei are described well by the calculations, then choosing one of the observables automatically leads to a poor (if any at all) description of the other, as can be seen from the plane-wave Born-approximation (PWBA) expression for the relation between charge density and form factor, which is simply a Fourier-Bessel transform [43]. Another problem with this procedure is that one usually fixes the occupancies in one of the nuclei (often to the IPSM values) and then varies the occupancies in the second nucleus. Since the occupancy difference to be deduced may quite well depend on the choice made for the occupancies of the first nucleus, this introduces an ambiguity. Furthermore, in fitting the charge-density difference, the problem with the error envelope of the experimental charge density becomes more acute as the uncertainty in the charge-density difference is usually quite large in the nuclear interior. Here, the incompleteness error is the dominant uncertainty and the uncertainty in the central part of the charge-density difference suffers from the incompleteness error of both nuclei.

In the present calculations, which are described below, a numerical fit of the occupancies to the experimental form-factor data of each nucleus has been performed. Subsequently, the influence of nuclear deformation on occupancies is investigated.

B. Present calculations

As the interest here is the $2s_{1/2}$-occupancy difference, its extraction will suffer from deviations between the calculated and actual s.p. $1s_{1/2}$ and $2s_{1/2}$ wave functions. It has been pointed out by Mahaux and Sartor [44] that the HF s.p. wave functions are only approximations to realistic wave functions. However, most aspects of nuclear structure do not change dramatically between adjacent nuclei. One might therefore expect discrepancies between the s.p. wave functions, and thus in the derived occupancies, to be roughly similar for adjacent nuclei, allowing for the extraction of an acceptable estimate for the $2s_{1/2}$-occupancy difference. The occupancies will depend on the type of (effective) nucleon-nucleon interaction used. The spread in occupancy differences, resulting from using several ''reasonable'' effective interactions, will give an estimate of the consistency of the interactions and the average value is expected to be a meaningful estimate of the true occupancy difference. It should be stressed that, as the quality of effective interactions is hard to assess, the fact that one of the interactions may give a better quality fit than others do does *not* imply anything about the quality of this interaction.

Apart from the HF calculations in a spherical basis (SHF), a set of Hartree-Fock calculations [45] has been performed in a deformed basis (DHF). In these calculations the s.p. wave functions are expanded into eigenfunctions of an axially symmetric deformed harmonic-oscillator potential. The degeneracy in the z component of the angular momentum is now lifted. The s.p. solutions for axially symmetric deformed nuclei are characterized by the eigenvalue of the third component of the total angular momentum and by the parity [45]. A state with a s.p. angular momentum $j=n/2$ now splits into components $k=1/2,3/2,\ldots,n/2$. Therefore, it is no longer appropriate to consider, for instance, only $1s_{1/2}$ or $2s_{1/2}$ transitions, but one must consider the sum of the $l=0$ strength originating from all $\frac{1}{2}^+$ projections. The energy separation between the different k components generally in-

creases with increasing deformation. The lifting of the degeneracy can result in a proton (neutron) configuration quite different from the one expected on the basis of the IPSM.

1. Spherically symmetric Hartree-Fock calculations

We have chosen to determine the occupancies via a numerical fit to the form-factor data. All spherically symmetric Hartree-Fock (SHF) calculations have been performed with the Mainz HF code [46]. First, a HF ground-state charge density is generated and from this HF form factors are calculated which are subsequently compared to the data. Next, the $2s_{1/2}$, $1d_{3/2}$, and $1f_{7/2}$ occupancies are varied, adjusting the occupancy for the $1d_{5/2}$ orbital to ensure a total proton number of Z, until the best possible description is obtained. Constraints can be set on occupancies to ensure that the resulting occupancies are realistic.

Effective Skyrme-type [47] interactions from several families of interactions have been used: the SkIII interaction [48], the G_σ interaction [49], the M^* interaction [50], the SkE2 and SkE4 interactions [51], and the FY1 interaction [52]. The SkE2/4 interactions differ from the previous three by the fact that they contain a momentum-dependent three-body term. The FY1 interaction is different from all other interactions in that it has a finite range for the T_0 term in the Skyrme parametrization with a Yukawa-type behavior. For the G_σ interaction also random-phase-approximation (RPA) ground-state correlations have been taken into account.

As the calculated nuclear properties depend on the specific interaction, it is necessary to discuss how the parameters in the interactions, mentioned above, have been obtained. Effective interactions are typically obtained from a fit of the interaction parameters to yield a good simultaneous description of binding energies, rms radii, etc., in a range of nuclei. More specifically, the parameters employed in the SkIII interaction have been obtained from a fit to binding energies and rms radii of the nuclei ^{16}O, ^{40,48}Ca, ^{56}Ni, ^{90}Zr, ^{140}Ce, and ^{208}Pb. A similar set of nuclei, extended with ^{114,132}Sn, was used to determine the parameters of the M^* interaction. Apart from the binding energy and the rms radius the height of the fission barrier in ^{240}Pu was also used to fit the parameters. The parameters of the two SkE interactions have been obtained from a fit of binding energies, rms radii and s.p. energies observed for the nuclei ^{16}O, ^{40,48}Ca, ^{90}Zr, ^{132}Sn, and ^{208}Pb. The two SkE interactions have different values of the Fermi momentum k_F. Both the G_σ and FY1 parameters have been fitted to binding energies and diffraction radii as well as surface thicknesses observed in ^{16}O, ^{40,48}Ca, ^{58}Ni, ^{90}Zr, ^{116,124}Sn, and ^{208}Pb. Furthermore, the LS splitting of the $1p$ level in ^{16}O was considered. Apart from the observables mentioned above, also the energies of the giant dipole resonance in ^{90}Zr, ^{116,124}Sn, and ^{208}Pb have been taken into account.

For the determination of the parameters in the Sk-a interaction binding energies and skin thicknesses in ^{40,48}Ca and ^{208}Pb were fitted. Furthermore, a good reproduction of various parameters in Myers and Swiatecki's mass formula [53] was required.

Although the main interest is in the occupancy-number difference between the two even-even nuclei ^{30}Si and ^{32}S, the calculations have also been performed for ^{31}P. The results obtained for this odd-even nucleus, however, should be treated with care.

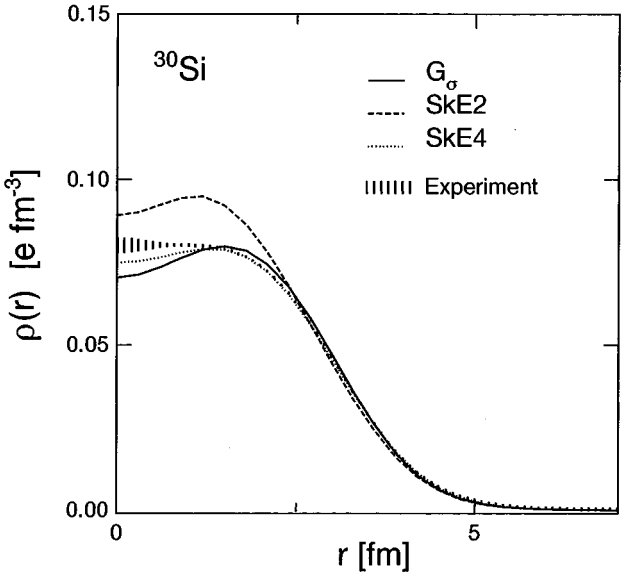

FIG. 5. Calculated ground-state charge distributions for ^{30}Si in a HF+BCS approach. The experimental distribution (hatched region) and the results obtained with the G_σ, SkE2, and SkE4 interactions are shown.

a. The nucleus ^{30}Si. In the IPSM limit the nucleus ^{30}Si has all proton orbitals filled up to and including the $1d_{5/2}$ orbital. From $(e,e'p)$ experiments [23] the $2s_{1/2}$ and, to a lesser extent, the $1d_{3/2}$ orbitals are known to be fractionally populated. In the present calculations, the occupancy of the $1d_{3/2}$ orbital was fixed at 0.20 protons, compatible with the results of a HF+BCS calculation with a pairing gap of 2.1 MeV. The distribution of the remaining protons over the $1d_{5/2}$ and $2s_{1/2}$ orbitals was adjusted to obtain the best description of the cross-section data. In the $(e,e'p)$ experiments no knockout from the $1f_{7/2}$ orbital was observed and therefore a possible occupancy of this orbital has not been considered. The neutron configuration was taken from a HF+BCS calculation. The influence of this configuration on the calculated form factors was found to be small, and it was therefore fixed to these values during the determination of the proton occupancies.

The SkE2 interaction is unable to give an acceptable description of the form-factor data. This is further illustrated in Fig. 5 where the experimental ground-state charge distribution of ^{30}Si is compared to results calculated in a straightforward HF+BCS approach with three of the interactions. Clearly, the shape of the ground-state charge distribution calculated with the SkE2 interaction is quite different from the other calculations and the data. A similar effect was observed for the other two nuclei. The SkE2 interaction was, therefore, not considered any further.

The calculated form-factor data, together with the fits, are shown in Fig. 6. The SkIII interaction fails to describe the form-factor data, even at moderately low momentum transfer. The other interactions all yield a good description of the form-factor data up to a q_{eff} value of roughly 2.3 fm^{-1}, the location of the second diffraction minimum. At higher q_{eff} values the calculations diverge. The G_σ and FY1 inter-

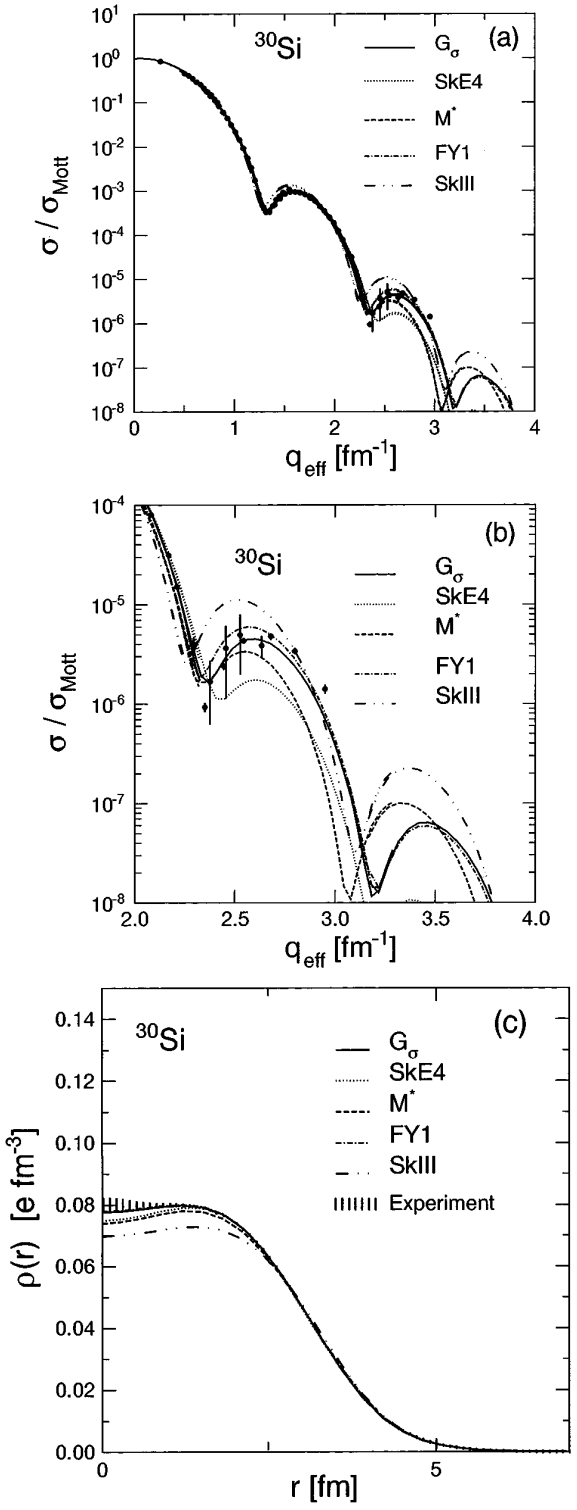

FIG. 6. (a) Form-factor data for ^{30}Si compared to the results of the spherically symmetric Hartree-Fock calculations. The results obtained with the G_σ, M^*, SkE4, FY1, and SkIII interactions are shown. (b) High-momentum-transfer part of the form-factor data for ^{30}Si compared to the results of the spherically symmetric Hartree-Fock calculations. The results obtained with the G_σ, M^*, SkE4, FY1, and SkIII interactions are shown. (c) Experimental ground-state charge distribution of ^{30}Si compared to the results of the spherically symmetric Hartree-Fock calculations. The results obtained with the G_σ, M^*, SkE4, FY1, and SkIII interactions are shown.

TABLE IV. Main results of the spherically symmetric Hartree-Fock calculations. The errors given in the experimental quantities are the statistical errors.

	FY1	G_σ	M^*	SkE4	SkIII	Expt.
^{30}Si						
$n_{1d_{5/2}}$	5.19(1)	5.24(1)	5.52(1)	5.33(1)	5.23(1)	
$n_{2s_{1/2}}$	0.61(1)	0.56(1)	0.28(1)	0.47(1)	0.57(1)	
$n_{1d_{3/2}}$	0.20	0.20	0.20	0.20	0.20	
$n_{1f_{7/2}}$	-	0.00	0.00	0.00	0.00	
E_{tot} [MeV]	246.93	246.23	251.11	237.98	245.41	255.62
r_{rms} [fm]	3.126	3.129	3.150	3.143	3.155	3.145(4)
^{31}P						
$n_{1d_{5/2}}$	5.76(7)	5.71(8)	5.74(4)	5.72(8)	5.16(7)	
$n_{2s_{1/2}}$	0.94(2)	0.93(1)	0.91(1)	0.92(1)	0.98(2)	
$n_{1d_{3/2}}$	0.30(5)	0.26(8)	0.25(4)	0.26(8)	0.76(7)	
$n_{1f_{7/2}}$	-	0.10	0.10	0.10	0.10	
E_{tot} [MeV]	255.63	255.12	259.10	246.35	252.22	262.92
r_{rms} [fm]	3.195	3.185	3.207	3.199	3.223	3.191(5)
^{32}S						
$n_{1d_{5/2}}$	5.89(3)	5.58(3)	5.69(12)	5.73(6)	6.00(4)	
$n_{2s_{1/2}}$	1.53(1)	1.49(1)	1.54(1)	1.41(1)	1.63(1)	
$n_{1d_{3/2}}$	0.58(3)	0.73(2)	0.57(12)	0.66(6)	0.17(4)	
$n_{1f_{7/2}}$	-	0.20	0.20	0.20	0.20	
E_{tot} [MeV]	263.00	259.54	263.43	257.50	261.67	271.78
r_{rms} [fm]	3.253	3.253	3.262	3.257	3.275	3.243(4)

actions yield a better description than the M^* and SkE4 interactions. A similar situation is found in r space: SkIII is completely off in describing the experimental ground-state charge distribution, and SkE4 and M^* show small deviations in the interior, while both G_σ and FY1 yield a good description.

The resulting occupancies and a number of calculated quantities such as the binding energy and rms radius of the ground-state charge distribution are listed in Table IV. The M^* and SkE4 interactions yield a value for the rms radius that is in agreement with the experimental value of 3.145(5) fm, whereas SkIII yields a slightly higher value, and FY1 and G_σ (which gave the best description to the form-factor data) yield a smaller value. Compared to the experimental binding energy [54] of 255.62 MeV or, alternatively, the binding energy per nucleon of 8.52 MeV, all calculations yield results that are too low.

b. The nucleus ^{31}P. As for ^{30}Si, preliminary calculations were performed to obtain an estimate of the occupancies. It was found that in this case the occupancy of the $1d_{3/2}$ orbital could be fitted, although the correlation between the occupancies of the $1d_{5/2}$ and $1d_{3/2}$ orbitals results in somewhat larger uncertainties in the resulting occupancies, due to the similarity in shape of the wave functions. Also some $1f_{7/2}$ strength was required; the best results were obtained with a (fixed) $1f_{7/2}$ occupancy of 0.1. Unfortunately, the model space of the computer code used to calculate the FY1 interaction did not include the $1f_{7/2}$ orbital. The results of the calculations for ^{31}P are shown in Fig. 7. As in ^{30}Si, the G_σ interaction gives a good description of the ex-

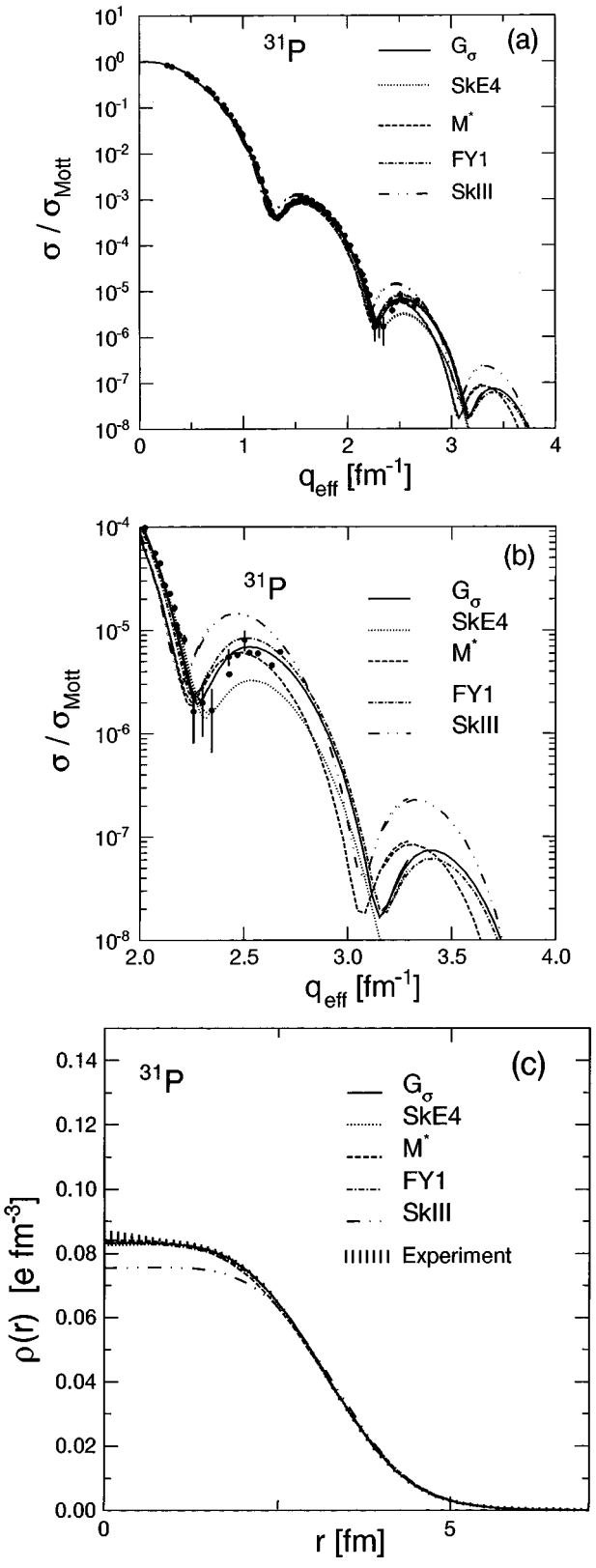

FIG. 7. (a) Same as Fig. 5(a) but for ^{31}P. (b) Same as Fig. 5(b) but for ^{31}P. (c) Same as Fig. 5(c) but for ^{31}P.

perimental data, in q space as well as in r space. Here too, the SkIII interaction fails completely and the SkE4 interaction underestimates the form factor for q_{eff} beyond the second diffraction minimum. The occupancies, rms radii, and binding energies are listed in Table IV.

c. The nucleus ^{32}S. For ^{32}S a fixed $1f_{7/2}$ occupancy of 0.2 was found to give reasonable results in the present calculations. The occupancies of the $1d_{5/2}$, $2s_{1/2}$, and $1d_{3/2}$ orbitals were adjusted to yield the best description of the form-factor data. While all calculations predict a third maximum around $q_{\text{eff}}=3.5$ fm^{-1} the data show a quite different behavior. Up to a q_{eff} of almost 3.0 fm^{-1}, the G_σ interaction gives a good description of the experimental data. Again the SkIII interaction fails to describe the data while both the SkE4 and FY1 interaction as well as the M^* interaction give intermediate results. Above 3.0 fm^{-1} all interactions, including the G_σ, fail to describe the behavior of the data. This is not surprising, since for this high q_{eff} the data have a large contribution from short-range correlations which are not incorporated in the mean-field picture. The results of the calculations are shown in Fig. 8. In r space all interactions except SkIII yield almost the same ground-state charge distribution, despite the relatively large differences between the calculated cross sections.

d. The form-factor ratio of ^{30}Si *and* ^{32}S. For completeness the form-factor ratio of ^{30}Si and ^{32}S was also fitted with the G_σ interaction; the results are shown in Fig. 9. Clearly, the quality of the description is quite good. To obtain this, values for the occupancies in ^{30}Si had to be chosen different from the IPSM configuration: 5.50, 0.35, and 0.15 protons in the $1d_{5/2}$, $2s_{1/2}$, and $1d_{3/2}$ orbitals, respectively. The occupancies in ^{32}S were then found to be 5.98, 1.15, 0.62, and 0.25 protons in the $1d_{5/2}$, $2s_{1/2}$, $1d_{3/2}$, and $1f_{7/2}$ orbitals, respectively. The $2s_{1/2}$ occupancy difference between the two nuclei thus obtained is equal to 0.8, low compared to the result from the calculations presented above and also low compared to the difference in ΣC^2S from the $(e,e'p)$ study [23].

2. Hartree-Fock calculations in a deformed basis

In the DHF calculations the occupancies were not adjusted but a self-consistent solution of the HF equations was searched for that has, simultaneously, a maximum binding energy and a stable deformation. Three different Skyrme-type interactions were used: the SkIII [48], Sk-a [55], and M^* [50]. The calculations were performed both without (DHF) and with (DHF+BCS) the inclusion of pairing correlations. It was observed that, as the energy gap is increased from 0 MeV to the values deduced from experimental mass differences (2.1, 2.0, and 2.1 MeV for ^{30}Si, ^{31}P, and ^{32}S, respectively), the calculated deformation becomes quite small, almost consistent with that of a spherical shape. This phenomenon is caused by the creation of $L=0$ pairs, which results in a decreased deformation.

The calculated values for the intrinsic quadrupole moments, binding energies, and deformation parameters for the non-BCS DHF calculations are listed in Table V. In Table VI the same quantities, as well as the resulting occupancies, are listed for the DHF+BCS calculations. Also listed in Tables V and VI are experimental quadrupole moments [56] and values for the deformation parameter derived from these.

a. The nucleus ^{30}Si. For ^{30}Si all three interactions resulted in values of the deformation β less than 0.07 for the non-BCS DHF calculations, where a value of β larger than

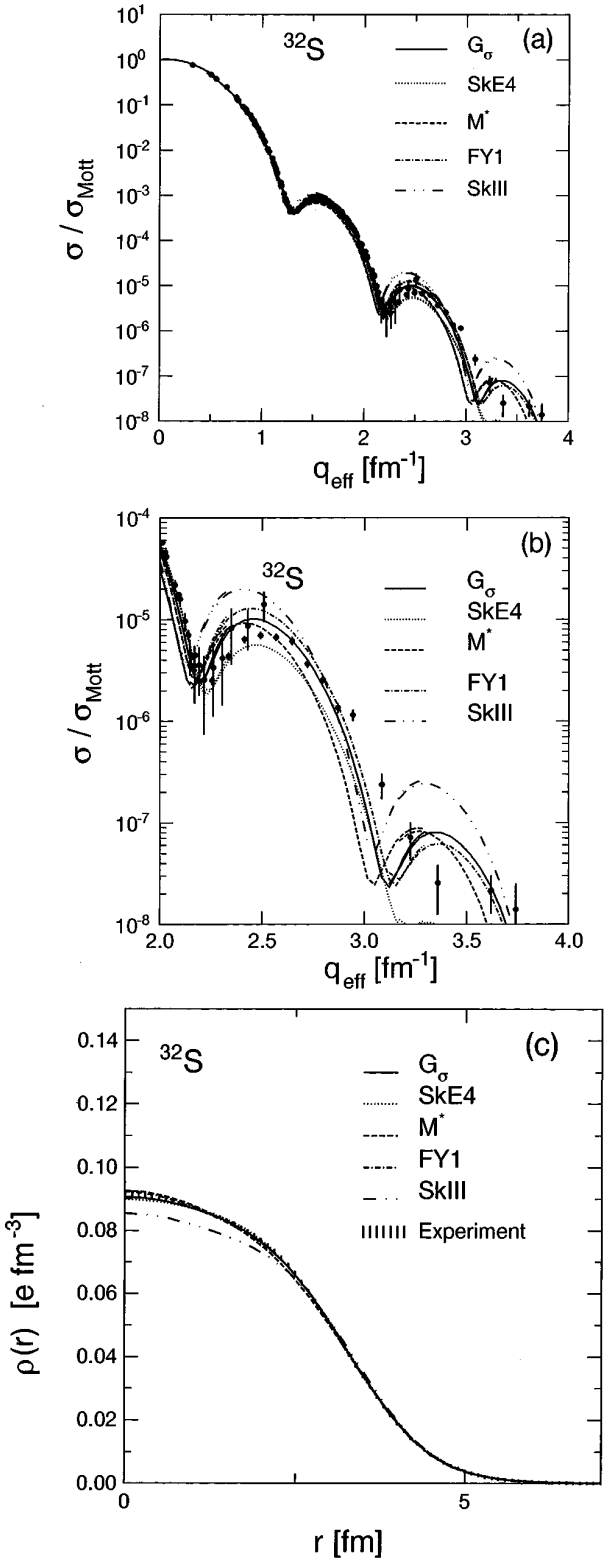

FIG. 8. (a) Same as Fig. 5(a) but for ^{32}S. (b) Same as Fig. 5(b) but for ^{32}S. (c) Same as Fig. 5(c) but for ^{32}S.

0.1 would indicate a significant deformation. Two experimental values for the intrinsic quadrupole moment (Q_0) are reported [56]: 17.5 e fm^2 and -3.5 e fm^2, both with an uncertainty of 21 e fm^2. It is therefore concluded that ^{30}Si is almost spherical. The M^* interaction gives a deformation

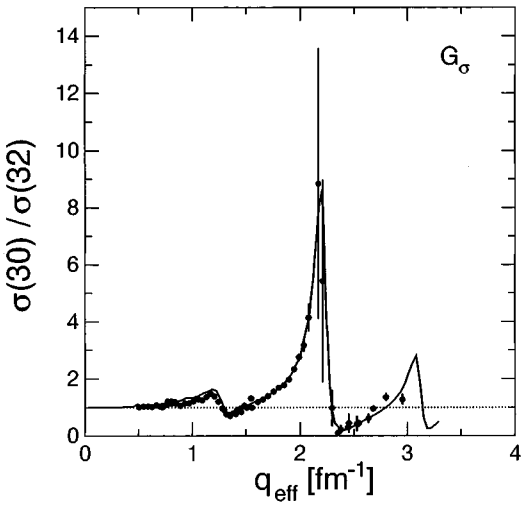

FIG. 9. The experimental form-factor ratio of ^{30}Si and ^{32}S compared to the ratio calculated using the G_σ interaction.

which is an order of magnitude smaller than the roughly similar deformations obtained with the SkIII and Sk-a interactions. In the DHF calculations the SkIII interaction and the Sk-a interaction yield values for Q_0 that are significantly larger than the value obtained with the M^* interaction, although all three results are consistent with experiment within the uncertainty. The binding energy is reasonably close to the experimental value [54] of 255.62 MeV, both in the DHF and DHF+BCS calculations. In Fig. 10 the (DHF+BCS) ground-state charge densities are shown as calculated with each of the three interactions. The SkIII interaction clearly underestimates the experimental density in the interior. This is to a lesser extent also true for the Sk-a interaction. The M^* interaction is somewhat more successful although in this case the experimental density is overestimated.

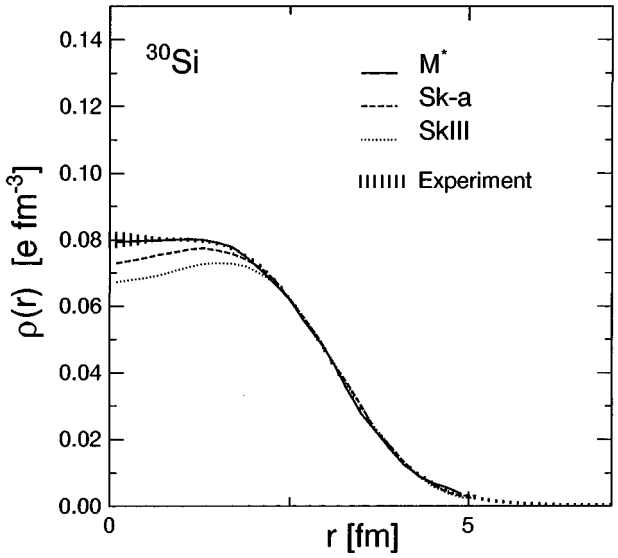

FIG. 10. Experimental ground-state charge density for ^{30}Si, compared to the densities obtained in the DHF+BCS calculations. The results calculated with the SkIII, Sk-a, and M^* interactions are shown.

TABLE V. Main results of the DHF calculations.

Nucleus	Observable	SkIII	Sk-a	M^*	Expt.
^{30}Si	$n_{k^\pi=5/2^+}$	5.94	5.97	6.00	
	$n_{k^\pi=1/2^+}$	2.04	2.02	2.00	
	$n_{k^\pi=3/2^+}$	0.01	0.01	0.00	
	$E_{\rm tot}$ [MeV]	253.67	250.32	259.03	255.62
	$r_{\rm rms}$ [fm]	3.147	3.142	3.119	3.145(4)
	Q_0 [e fm^2]	11.06	7.57	0.74	-3.5(21.0)/17.5(21.0)
	β	0.069	0.044	0.004	-0.019(117)/0.097(117)
^{31}P	$n_{k^\pi=5/2^+}$	5.81	5.81	6.00	
	$n_{k^\pi=1/2^+}$	2.63	2.74	3.00	
	$n_{k^\pi=3/2^+}$	0.52	0.42	0.00	
	$E_{\rm tot}$ [MeV]	260.02	257.44	266.78	262.92
	$r_{\rm rms}$ [fm]	3.251	3.247	3.198	3.191(5)
	Q_0 [e fm^2]	34.6	31.9	0.59	-
	β	0.191	0.174	0.003	-
^{32}S	$n_{k^\pi=5/2^+}$	5.88	5.90	6.00	
	$n_{k^\pi=1/2^+}$	3.01	3.30	4.00	
	$n_{k^\pi=3/2^+}$	0.98	0.78	0.00	
	$E_{\rm tot}$ [MeV]	267.77	265.33	274.34	271.78
	$r_{\rm rms}$ [fm]	3.281	3.284	3.238	3.243(4)
	Q_0 [e fm^2]	41.7	37.9	0.68	40(7)/63(26)
	β	0.200	0.182	0.003	0.190(33)/0.299(123)

TABLE VI. Main results of the DHF+BCS calculations.

Nucleus	Observable	SkIII	Sk-a	M^*	Expt.
^{30}Si	$n_{k^\pi=5/2^+}$	5.42	5.39	5.33	
	$n_{k^\pi=1/2^+}$	2.31	2.36	2.46	
	$n_{k^\pi=3/2^+}$	0.18	0.16	0.12	
	$E_{\rm tot}$ [MeV]	254.68	251.11	259.89	255.62
	$r_{\rm rms}$ [fm]	3.165	3.171	3.150	3.145(4)
	Q_0 [e fm^2]	3.00	5.31	0.74	-3.5(21.0)/17.5(21.0)
	β	0.018	0.030	0.004	-0.019(117)/0.097(117)
^{31}P	$n_{k^\pi=5/2^+}$	5.63	5.66	5.68	
	$n_{k^\pi=1/2^+}$	2.97	3.00	3.00	
	$n_{k^\pi=3/2^+}$	0.28	0.26	0.18	
	$E_{\rm tot}$ [MeV]	261.80	258.94	268.05	262.92
	$r_{\rm rms}$ [fm]	3.243	3.249	3.225	3.191(5)
	Q_0 [e fm^2]	8.06	4.06	0.93	-
	β	0.042	0.021	0.005	-
^{32}S	$n_{k^\pi=5/2^+}$	5.81	5.81	5.81	
	$n_{k^\pi=1/2^+}$	3.15	3.35	3.49	
	$n_{k^\pi=3/2^+}$	0.82	0.68	0.44	
	$E_{\rm tot}$ [MeV]	269.37	266.60	275.55	271.78
	$r_{\rm rms}$ [fm]	3.273	3.288	3.263	3.243(4)
	Q_0 [e fm^2]	3.46	4.34	1.07	40(7)/63(26)
	β	0.017	0.021	0.005	0.190(33)/0.299(123)

The DHF calculations for all interactions severely underestimate the experimental density in the interior. The total $\frac{1}{2}^+$ strength is close to 2 for all interactions. Furthermore, we have seen that ^{30}Si is almost spherical. This implies that all DHF calculations predict an almost empty $2s_{1/2}$ orbital, resulting in a rather low density in the interior, in contrast with the experimental observation.

b. The nucleus ^{31}P. For ^{31}P results quite similar to ^{30}Si are obtained. In the DHF calculations the SkIII and Sk-a interactions result in sizable values of β. The calculated binding energies are quite close to the experimental value [54] of 262.92 MeV. The main results of the two sets of calculations are listed in Tables V and VI. Experimental and calculated (DHF+BCS) ground-state charge densities are shown in Fig. 11. The densities calculated with the SkIII and Sk-a interactions agree to a large extent with the experimental data; especially, the Sk-a curve is quite good. Unfortunately, no experimental values are available for the (intrinsic) quadrupole moment of ^{31}P.

c. The nucleus ^{32}S. For this nucleus several experimental values [56] are known for the intrinsic quadrupole moment, ranging from 40(7) $e\,\mathrm{fm}^2$ to 63(26) $e\,\mathrm{fm}^2$. The non-BCS DHF calculations yield (except for the calculation with the M^* interaction) values for Q_0 that are within the experimental uncertainty. All DHF+BCS calculations result in values for Q_0 that are too low by almost an order of magnitude. The binding energy for ^{32}S calculated with the M^* interaction is quite poor compared to the experimental value [54] of 271.78 MeV. Both of the other interactions give a good reproduction in the DHF case and values that are somewhat too low for the DHF+BCS calculations. Interestingly, the M^* interaction is the only one that gives a reasonable description of the experimental ground-state charge distribution. Experimental and calculated (DHF+BCS) ground-state charge densities are shown in Fig. 12.

3. Comparison

A comparison of the two sets of HF calculations immediately shows some differences. Whereas the SHF calculations

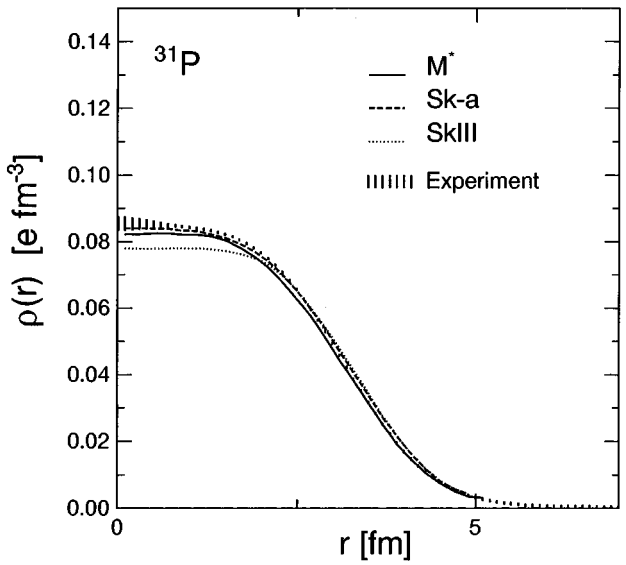

FIG. 11. Same as Fig. 10 but for ^{31}P.

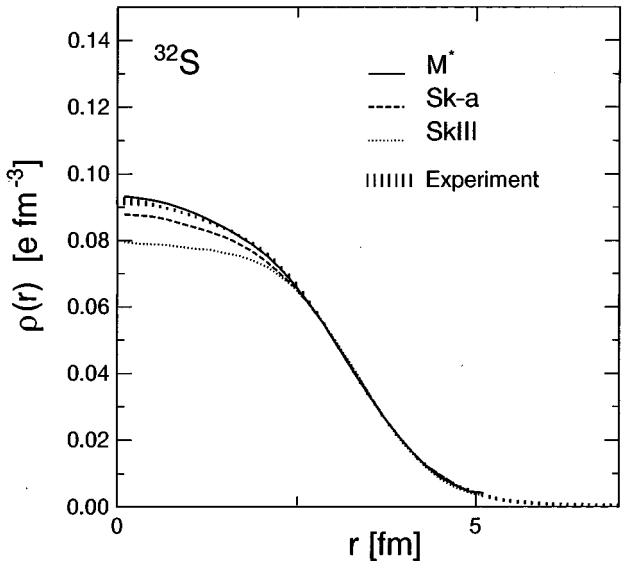

FIG. 12. Same as Fig. 10 but for ^{32}S.

yield acceptable to good descriptions of the form-factor data, and generally also of the ground-state charge densities, they result in binding energies that are up to 10 MeV too low. The latter effect had already been observed in a previous study of sd-shell nuclei [20]. The DHF and DHF+BCS calculations yield rather the opposite results: The calculated binding energies are closer to the experimental values whereas almost all of the calculations underestimate the ground-state charge densities by a sizable amount. It is, however, satisfying that the spread in $2s_{1/2}$-occupancy differences is not large.

In the DHF calculations the M^* interaction leads in all three nuclei, regardless of the pairing, to a proton configuration that is quite like the IPSM configuration. As a result the calculated values for the deformation parameter β are quite close to zero. The other two interactions result in sizable values of the deformation in the DHF calculations and, to a lesser extent, in the DHF+BCS calculations. In view of the large experimental value for the intrinsic quadrupole moment for ^{32}S it is concluded that the M^* interaction is not suitable for this type of calculations.

In general it is observed that the total binding energy does not change by a significant amount when pairing correlations are included in the calculation by means of a BCS approach. Whereas the non-BCS calculations yield a deformation that is quite reasonable, the inclusion of pairing immediately decreases the equilibrium deformation to a level that is much too low with respect to experimental data for ^{32}S. This may indicate that both effects, nuclear deformation and pairing correlations, should be treated on a much more equal footing.

IV. OCCUPANCY DIFFERENCES AND SPECTROSCOPIC STRENGTHS

As pointed out in the Introduction, the occupancies obtained from HF calculations have to be viewed with caution. Although they are expected to represent a reasonable approximation of the ''real'' occupancies, several effects, e.g., short-range correlations and core polarization, are not taken into account. For short-range correlations of the Jastrow type

it has been shown [57] that the effects do not change noticeably in going from nucleus A to nucleus $A+1$ or $A+2$. In comparing two neighboring even-even nuclei it is also not unreasonable to assume the core polarization to be of the same order. Therefore, the difference in calculated occupancies is assumed to be more reliable.

In $(e,e'p)$ experiments one measures the spectroscopic strength [58]. Here, one is confronted with the possibility that not all strength is contained in the experimentally covered energy range [3,7]. On grounds similar to those discussed above one expects that in the ratio of spectroscopic strengths obtained for nucleus A and nucleus $A+2$ this unobserved strength largely cancels. Possible imperfections in the optical-model potential, used to account for the distortion of the outgoing proton in the field of the residual nucleus, are also expected to cancel to a large extent when taking the ratios. With the aid of a theorem by French and MacFarlane [14], later extended in a general theory of overlap functions by Clement [15], the spectroscopic strength ratio can be related directly to the ratio of occupancies. In this procedure the total summed spectroscopic strength observed for knockout from a specific orbital is assumed to converge, by integrating to high excitation energies, to the number of particles in this orbital (the occupancy). If long- and short-range correlations are similar in two nuclei, then it is expected that the spectroscopic strength observed in the experimentally accessible energy range converges to the same fraction of the total spectroscopic strength. The ratio of summed spectroscopic strengths is then assumed to be equal to the ratio of occupancies for these same orbitals.

A set of $(e,e'p)$ experiments has been performed, the results of which have been published separately [23]. One can combine the occupancy differences between ^{30}Si and ^{32}S obtained in the present paper with the occupancy ratio as deduced from the $(e,e'p)$ experiments. A similar procedure has been applied in the $3s_{1/2}$ shell [13,16,17] in the Pb region. The application of the CERES method in the case of the $3s_{1/2}$ orbital relies heavily on the contribution of the s.p. $3s_{1/2}$ proton density to the calculated HF ground-state charge density. The experimental charge-density difference is compared to the density distribution of a $3s_{1/2}$ proton. In this approach differences between the $3s_{1/2}$ density in ^{205}Tl and ^{206}Pb are ignored. It has been remarked by Mahaux and Sartor [44] that this approach is questionable. Furthermore, this experiment relied on a comparison between an even-even nucleus with one of odd A. As has been remarked before concerning the nucleus ^{31}P, the results might be less reliable than for a case where two even-even nuclei are compared.

From the occupancy differences obtained in both the spherical and the deformed (plus BCS) calculations, ''absolute occupancies'' can be calculated. For the deformed HF calculations the $s_{1/2}$ occupancy difference is attributed to the $2s_{1/2}$ occupancy difference. Because the true nucleon-nucleon interaction is not known and the effective interaction giving the best fit to some observable is not necessarily the ''best'' approximation to the ''real'' nucleon-nucleon interaction, all occupancy differences obtained in the two sets of calculations described above have been considered. The experimentally deduced [23] values of 0.23(3) and 1.29(13) for the summed $2s_{1/2}$ spectroscopic strengths in ^{30}Si and ^{32}S, respectively, resulted in the following values for the $2s_{1/2}$ occupancy numbers: $n_{30}=0.23(6)$ and $n_{32}=1.28(26)$ protons, respectively. These numbers have been obtained by taking the smallest and largest occupancy-number difference obtained in the SHF and DHF+BCS calculations and subsequently calculating the occupancies.

Although the HF results for the odd-even nucleus ^{31}P should be treated with caution, it is nevertheless instructive to deduce the $2s_{1/2}$ occupancy for this nucleus. With the summed $2s_{1/2}$ spectroscopic strength [23] for ^{31}P of 0.69(5) and the occupancy difference between ^{30}Si and ^{31}P of 0.54(14) proton, $2s_{1/2}$ occupancies of 0.27(9) and 0.81(21) protons for ^{30}Si and ^{31}P, respectively, are obtained. The $2s_{1/2}$ occupancy difference between ^{31}P and ^{32}S of 0.42(24) proton results in occupancies of 0.89(53) and 0.47(31) protons for ^{32}S and ^{31}P, respectively. The occupancies derived for each nucleus are consistent with each other within the uncertainties.

V. DISCUSSION

Some remarks should be made concerning the interpretation of the results for the occupancies, extracted in the previous section. The uncertainties in the final results can be reduced somewhat by noting that the summed spectroscopic strengths, which are used as input into the procedure, are lower limits to the occupancies. One can then assume the actual occupancies to be between the lower limit of the spectroscopic factor and the upper limit of the uncertainty of the occupancy, derived before. For the nuclei ^{30}Si and ^{32}S this results in $2s_{1/2}$ occupancies of 0.24(4) and 1.35(19), respectively.

Several assumptions are used in deriving the occupancies. One of them is that short-range correlations, responsible for the spreading of strength over a wide energy range, are roughly the same for both nuclei. If this is not the case, the ratio of summed spectroscopic strengths is not equal to the ratio of occupancies, and thus the derived occupancies are incorrect. It should be noted, however, that rather large effects introduce only small changes in the deduced occupancies. For example, if the present value for the ratio is assumed to change by 10%, the values for the derived $2s_{1/2}$ occupancies for ^{32}S and ^{30}Si change by only 0.04. Compared to the overall uncertainty this is a small effect, especially for ^{32}S.

The main cause of the uncertainties in the occupancies is the spread in calculated occupancy differences. From Sec. III it may be clear that the choice of the best effective interaction is not trivial. The SHF calculations yield a strong preference for the G_σ interaction, due to its good description of elastic form-factor data. Binding energies calculated with this interaction are, however, systematically too low. This effect was already noted by Friedrich and Reinhard [49] in parametrizing this interaction. The relatively good description of the form-factor data by the G_σ and FY1 interactions is probably due to the fact that they have been fitted to, among others, diffraction radii and surface thicknesses. Although the binding energies calculated in the DHF approach are closer to the experimental values, the ground-state charge densities, and thus the elastic form-factor data, are not reproduced well.

TABLE VII. $2s_{1/2}$ occupancies derived for ^{30}Si, ^{31}P, and ^{32}S.

^{30}Si	^{31}P	^{32}S
0.23(6)		1.28(26)
0.27(9)	0.81(21)	
	0.47(31)	0.89(53)

TABLE VIII. As in Table VII, but now with lower limits enforced by the available $(e,e'p)$ spectroscopic factors (see text).

^{30}Si	^{31}P	^{32}S
0.24(5)		1.35(19)
0.28(8)	0.86(17)	
	0.74(5)	1.35(9)

The precise neutron and proton configurations assumed for nuclei used in the determination of effective-force parameters influence the results. Interactions fitted to nuclei with an assumed IPSM configuration are not able to reproduce binding energies, rms radii, etc., once the IPSM assumption is dropped. This might explain why interactions such as the SkIII interaction result in a poor overall agreement between experimental and calculated observables.

VI. CONCLUDING REMARKS

In this paper we have presented elastic form-factor data to extend the available data sets for ^{30}Si and ^{31}P. In a combined analysis of all available data we have accurately deduced the ground-state charge density and the rms radius for ^{30}Si, ^{31}P, and ^{32}S. Combined with the existing data sets for these nuclei the elastic form-factor data have served as input for an extensive set of HF calculations. The effects of employing different effective nucleon-nucleon interactions in these HF calculations have been studied and $2s_{1/2}$ occupancy differences ^{32}S$-^{30}$Si, ^{31}P$-^{30}$Si, and ^{32}S$-^{31}$P have been obtained. The use of an interaction with a (partial) finite-range character, such as the FY1 interaction, does not lead to results that are fundamentally different from those obtained with pure zero-range interactions, for both ^{30}Si and ^{32}S. The HF $2s_{1/2}$ occupancies obtained in the SHF calculations for ^{30}Si are, apart from those derived with the M^* interaction, a factor of 2 higher than the occupancies for this orbital obtained in the $(e,e'p)$ analysis. The occupancies obtained in the DHF calculations are closer to the experimental ones. For ^{31}P the SHF and DHF results for the $2s_{1/2}$ occupancy are some 20% higher than the experimental values. The $2s_{1/2}$ occupancies obtained in the SHF calculations for ^{32}S are, again, roughly 20% too high whereas the occupancies obtained in the DHF calculations are roughly comparable to the experimental ones. In the DHF+BCS calculations it was observed that it was not possible to obtain a realistic equilibrium deformation.

Combining the occupancy number differences with previous $(e,e'p)$ data has allowed to calculate $2s_{1/2}$ occupancies in all three nuclei, as listed in Tables VII and VIII. The two sets of calculations, in a spherical basis and in a deformed basis, yield roughly comparable results for the occupancy differences, although neither yields a simultaneous good description of both the elastic form-factor data and the binding energies. With the lower limit, enforced by the available spectroscopic factors, the uncertainties in the occupancies have been reduced. The main uncertainty, apart from the choice of the interaction, is the influence of short-range correlations. It was illustrated in Sec. V that for ^{32}S this uncertainty is probably relatively small, of the order of 3%. It is clearly of paramount importance to obtain a better understanding of the way nucleons interact, especially when both nuclear deformation and pairing correlations are important, before more meaningful occupancy numbers can be obtained.

ACKNOWLEDGMENTS

We would like to thank J. Friedrich and D. Van Neck for fruitful discussions. We also wish to thank Joann Millikine of the U.S. Naval Research Laboratory for providing access to a helium glovebox for fabrication of the Li_2S targets. This work is part of the research program of the National Institute for Nuclear Physics and High-Energy Physics (NIKHEF), made possible by financial support from the Foundation for Fundamental Research on Matter (FOM) and the Netherlands' Organization for Scientific Research (NWO) and by the U.S. National Science Foundation under Grant No. PHY 89-21146.

[1] T.W. Donnelly, in *Symmetries in Nuclear Structure*, edited by K. Abrahams, K. Allaart, and A.E.L. Dieperink (Plenum, New York, 1983), p. 1.

[2] G.J. Kramer, Ph.D. thesis, University of Amsterdam, Amsterdam, The Netherlands, 1990.

[3] P.K.A. de Witt Huberts, J. Phys. G **16**, 507 (1990).

[4] J.W.A. den Herder, Ph.D. thesis, University of Amsterdam, Amsterdam, The Netherlands, 1987; J.W.A. den Herder, H.P. Blok, E. Jans, P.H.M. Keizer, L. Lapikás, E.N.M. Quint, G. van der Steenhoven, and P.K.A. de Witt Huberts, Nucl. Phys. **A490**, 507 (1988).

[5] G. van der Steenhoven, H.P. Blok, E. Jans, M. de Jong, L. Lapikás, E.N.M. Quint, and P.K.A. de Wit Huberts, Nucl. Phys. **A480**, 547 (1988).

[6] C. Giusti and F.D. Pacati, Nucl. Phys. **A473**, 717 (1987); J.P. McDermott, Phys. Rev. Lett. **65**, 199 (1991).

[7] L. Lapikás, in *Electron Scattering: Past and Future*, Proceedings of the 6th Amsterdam miniconference, Amsterdam, The Netherlands, 1989, edited by C. W. de Jager, L. Lapileás, and H. deVries (CWI, Amsterdam, 1989), p. 81.

[8] V.R. Pandharipande, Nucl. Phys. **A497**, 43c (1989).

[9] O. Benhar, A. Fabrocini, and S. Fantoni, Nucl. Phys. **A505**, 267 (1989).

[10] D. Van Neck, M. Waroquier, and J. Ryckebusch, Nucl. Phys. **A530**, 347 (1991).
[11] C. Mahaux and R. Sartor, Nucl. Phys. **A484**, 205 (1988).
[12] C. Mahaux and R. Sartor, Nucl. Phys. **A503**, 525 (1989).
[13] P. Woldt, P. Grabmayr, G. Rau, G.J. Wagner, M.A. Hofstee, J.M. Schippers, S.Y. van der Werf, and H. Nann, Nucl. Phys. **A518**, 496 (1990), and references therein; P. Grabmayr, Prog. Part. Nucl. Phys. **29**, 251 (1992).
[14] J.B. French and M.H. MacFarlane, Nucl. Phys. **26**, 168 (1961).
[15] C.F. Clement, Nucl. Phys. **A213**, 469 (1973).
[16] J.M. Cavedon, B. Frois, D. Goutte, M. Huet, Ph. Leconte, C.N. Papanicolas, S.-H. Phan, S.K. Platchkov, S. Williamson, W. Boeglin, and I. Sick, Phys. Rev. Lett. **49**, 978 (1982).
[17] I. Sick and P.K.A. de Witt Huberts, Comments Nucl. Part. Phys. **20**, 177 (1991).
[18] J. Friedrich, Phys. Rev. C **33**, 2215 (1986).
[19] A.J.C. Burghardt, Ph.D. thesis, University of Amsterdam, Amsterdam, The Netherlands, 1989.
[20] G. Ripka, Adv. Nucl. Phys. **1**, 183 (1968).
[21] H. Überall, *Electron Scattering from Complex Nuclei* (Academic Press, New York, 1971), Pt. A, p. 170.
[22] B. Castel, I.P. Johnstone, B.P. Singh, and J.C. Parikh, Nucl. Phys. **A157**, 137 (1970).
[23] J. Wesseling, C.W. de Jager, L. Lapikás, H. de Vries, M.N. Harakeh, N. Kalantar-Nayestanaki, L.W. Fagg, R.A. Lindgren, and D. Van Neck, Nucl. Phys. **A547**, 519 (1992).
[24] C. de Vries, C.W. de Jager, L. Lapikás, G. Luijckx, R. Maas, H. de Vries, and P.K.A. de Witt Huberts, Nucl. Instrum. Methods Phys. Res. A **223**, 1 (1984).
[25] W. Reuter, G. Fricke, K. Merle, and H. Miska, Phys. Rev. C **26**, 806 (1982).
[26] E.A.J.M. Offermann, C.W. de Jager, and H. de Vries, Nucl. Instrum. Methods Phys. Res. A **262**, 298 (1987).
[27] J. Kelly (private communication).
[28] K. Merle, Ph.D. thesis, University of Mainz, Mainz, Germany, 1976.
[29] B. Dreher, J. Friedrich, K. Merle, H. Rothhaas, and G. Lührs, Nucl. Phys. **A235**, 219 (1974).
[30] H. Miessen, Ph.D. thesis, University of Mainz, Mainz, Germany, 1983.
[31] B.B.P. Sinha, G.A. Peterson, G.C. Li, and R.R. Whitney, Phys. Rev. C **6**, 1657 (1972).
[32] D. Rychel, H.J. Emrich, H. Miska, R. Gyufko, and C.A. Wiedner, Phys. Lett. **130B**, 5 (1983); D. Rychel, Ph.D. thesis, University of Mainz, Mainz, Germany, 1983.
[33] G.C. Li, M.R. Yearian, and I. Sick, Phys. Rev. C. **9**, 1861 (1974).
[34] G. Fricke, J. Herberz, Th. Hennemann, G. Mallot, L.A. Schaller, L. Schellenberg, C. Piller, and R. Jacot-Guillarmod, Phys. Rev. C **45**, 80 (1992).
[35] E.A.J.M. Offermann, L.S. Cardman, C.W. de Jager, H. Miska, C. de Vries, and H. de Vries, Phys. Rev. C **44**, 1096 (1991).
[36] L.A. Schaller, D.A. Barandao, P. Bergem, M. Boschung, T.Q. Phan, G. Piller, A. Rüetschi, L. Schellenberg, H. Schneuwly, G. Fricke, G. Mallot, and H.G. Sieberling, Phys. Rev. C **31**, 1007 (1985).
[37] G. Backenstoss, S. Charalambus, H. Daniel, H. Koch, G. Poelz, H. Schmitt, and L. Tauscher, Phys. Lett. **25B**, 547 (1967).
[38] D.R. Hartree, Proc. Camb. Philos. Soc. **24**, 89 (1928).
[39] V.A. Fock, Z. Phys. **61**, 126 (1930).
[40] A. deShalit and H. Feshbach, *Theoretical Nuclear Physics* (Wiley & Sons, New York, 1974), Vol. 1, and references therein.
[41] P. Ring and P. Schuck, *The Nuclear Many-Body Problem* (Springer, New York, 1980), and references therein.
[42] K. Heyde, *The Nuclear Shell Model* (Springer, Berlin, 1990), and references therein.
[43] T. de Forest, Jr., and J.D. Walecka, Adv. Phys. **15**, 1 (1966).
[44] C. Mahaux and R. Sartor, Adv. Nucl. Phys. **20**, 1 (1991).
[45] E. Moya de Guerra, P. Sarriguren, J.A. Caballero, M. Casas, and D.W.L. Sprung, Nucl. Phys. **A529**, 68 (1991).
[46] J. Friedrich and P.-G. Reinhard (private communication).
[47] T.H.R. Skyrme, Philos. Mag. **1**, 1043 (1956).
[48] F. Beiner, H. Flocard, N. Van Giai, and P. Quentin, Nucl. Phys. **A238**, 29 (1975).
[49] J. Friedrich and P.-G. Reinhard, Phys. Rev. C **33**, 335 (1986).
[50] J. Bartel, P. Quentin, M. Brack, C. Guet, and H.-B. Hakansson, Nucl. Phys. **A386**, 79 (1982).
[51] M. Waroquier, K. Heyde, and G. Wenes, Nucl. Phys. **A404**, 269 (1983).
[52] P.-G. Reinhard, A.S. Umar, K.T.R. Davies, M.R. Strayer, and S.-J. Lee, Phys. Rev. C **37**, 1026 (1988).
[53] W.D. Myers and W.J. Swiatecki, Ann. Phys. (N.Y.) **55**, 395 (1969); **84**, 186 (1974).
[54] A.H. Wapstra and G. Audi, Nucl. Phys. **A432**, 1 (1985).
[55] H.S. Köhler, Nucl. Phys. **A258**, 301 (1976).
[56] P. Raghavan, At. Data Nucl. Data Tables **42**, 189 (1989).
[57] M.C. Birse, and C.F. Clement, Nucl. Phys. **A351**, 112 (1981).
[58] S. Frullani and J. Mougey, Adv. Nucl. Phys. **14**, 1 (1984).